Available online at www.sciencedirect.com

ScienceDirect

journal homepage: www.elsevier.com/locate/he

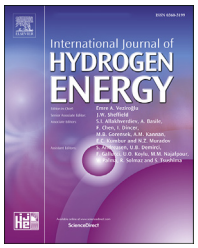

# Study of hydrogen storage properties of oxygen modified Ti- based $AB_2$ type metal hydride alloy

M.W. Davids [a,*], T. Martin [a], M. Lototskyy [a], R. Denys [b], V. Yartys [c]

[a] HySA Systems Competence Centre, South African Institute for Advanced Materials Chemistry (SAIAMC), University of the Western Cape, Bellville, South Africa
[b] HYSTORSYS AS, Kjeller, Norway
[c] Institute for Energy Technology, Kjeller, Norway

## HIGHLIGHTS

- Ti – based AB2 alloys synthesized by arc melting.
- Modification of Ti – based AB2 alloy by oxygen.
- MH alloy with relatively high reversible $H_2$ storage capacity (1.6 wt %).
- Improvement of hydrogen absorption kinetics of Ti – based AB2 alloy by addition of oxygen.

## ARTICLE INFO

*Article history:*
Received 10 March 2020
Received in revised form
21 May 2020
Accepted 23 May 2020
Available online 24 June 2020

*Keywords:*
Metal hydrides
$AB_2$
Arc melting
Oxygen modification
PCT properties
Activation
Kinetics

## ABSTRACT

A multi component $AB_2$ type hydrogen storage intermetallic alloy (A = $Ti_{0.85}Zr_{0.15}$, $B_2$ = $Mn_{1.22}Ni_{0.22}Cr_{0.2}V_{0.3}Fe_{0.06}$; was investigated in this work. The intermetallic specified above was modified by oxygen to yield the composition $AB_2O_{0.05}$. The oxygen was introduced by adding $TiO_2$ to the charge, with corresponding decrease of the Ti amount, followed by arc melting and annealing at the same conditions as for the oxygen free $AB_2$-type alloy. The addition of oxygen to the alloy did not change much the PCT properties; the only difference was that the plateau pressure for the oxygen-modified alloy increased slightly. Both alloys have shown to be excellent candidates for $H_2$ storage, particularly for utility vehicles, due to their relatively high reversible $H_2$ storage capacity (1.6 wt%) and low plateau pressure at room temperature (<5 bar). The addition of oxygen improved hydrogen absorption kinetics in the $AB_2$ alloy allowing it to immediately absorb $H_2$ without activation while for the non-modified sample an incubation period (30 min) was observed at the same conditions.



## Introduction

A promising application for metal hydrides as materials for hydrogen storage and source to Proton Exchange Membrane Fuel Cells (PEMFC's) is in specialized utility vehicles such as forklifts, mining locomotives and marine application. The low gravimetric hydrogen storage capacity and high weight of intermetallic hydrides can be beneficial as it assists in steadying the vehicle or vessel without carrying extra

* *Corresponding author.*
E-mail address: mwdavids@uwc.ac.za (M.W. Davids).
https://doi.org/10.1016/j.ijhydene.2020.05.215

counterweight [1–3]. Of the numerous metal hydride materials Ti- based $AB_2$ type (A = Ti+Zr; B = Mn+Cr+V+Fe+Ni+…) alloys have shown to be excellent hydrogen storage materials due to the relatively high reversible hydrogen storage capacity (~1.8 wt%) at near ambient conditions [4–6]. However one of the main drawbacks of Ti-based $AB_2$ alloys that hinders their commercial application is the high cost of raw materials. One of the technological challenges facing the everyday application of mass production of multi component Ti- based $AB_2$ type metal hydrides is the use of expensive elements. An operative method is to reduce the cost of Ti- based $AB_2$ alloys are to substitute pure V with inexpensive raw material such as ferrovanadium (FeV). Taizhong et al. reported on the synthesis of $TiCr_{1.8-x}(FeV)_x$ metal hydrides, the alloys showed excellent hydrogen storage capacities comparable to use of V metal [7]. Kim et al. reported on the synthesis of a $Ti_{0.85}Zr_{0.13}(FeV)_{0.56}Mn_{1.47}Ni_{0.05}$ alloy, they showed that the as-cast alloy consisted of two phases: a C14 Laves phase and a FeO phase. The source of the FeO phase in the alloy was attributed mainly due to the replacement of pure V by FeV. To remove the FeO phase, the alloy was annealed at 1000 °C for 1 h in Ar atmosphere that resulted in a single C14 Laves phase [8]. Sakaki et al. reported on TiZrMn alloy for the application as metal hydride actuators [9]. Their results illustrated that FeV could be used to reduce the cost of the alloy, and whereas the Al impurity in FeV assisted in decreasing hysteresis.

Numerous studies on Ti- based $AB_2$ alloys have been carried out in order to improve the performance of the alloy such as the storage capacity, cyclic stability, kinetics and activation which are normally achieved by substitution with different alloying elements [10–14]. The effects of oxygen in Ti-based alloys have been studied by various researchers, they concluded that even small amounts of oxygen affect the P–C isotherms, predominantly the dissociation pressure; the hydrogen storage capacities decrease and the plateau pressures of the alloys increase with increased oxygen concentration [15–17].

Introduction of oxygen in the alloys of Ti and/or Zr with transition metals (TM = Fe, V, Ni, etc.) often results in the formation of oxygen-stabilised intermetallic η-phases, $\eta_1$-$(Ti,Zr)_3TM_3O_{1-x}$ and $\eta_2$-$(Ti,Zr)_4TM_2O_{1-x}$ with crystal structures related to $Ti_2Ni$ [18–22]. These phases often form hydrides which, however, are characterised by high stabilities thus reducing reversible hydrogen storage capacity of the material at pressure-temperature conditions specific for the applications.

This paper reports on the synthesis and characterization of a multi component Ti-based $AB_2$ type alloy without ($AB_2$) and with ($AB_2O_{0.05}$) oxygen modification.

## Experimental

A multi component Ti based $AB_2$-type alloy with a composition of (A = $Ti_{0.85}Zr_{0.15}$, B = $Mn_{1.22}Ni_{0.22}Cr_{0.2}V_{0.3}Fe_{0.06}$) was prepared by arc-melting of the starting elements (metals of >99.99% purity; V and Fe were introduced as commercial Ferrovanadium/FeV, 80 wt% V) in stoichiometric ratios. The total weight of ingots was about 10 g. The melting was performed on a water-cooled copper hearth in Ar atmosphere (99.999%; pressure 0.1 MPa). The alloys were re-melted 3 times to guarantee their homogeneity. The as-cast alloy was sealed in a stainless steel tube filled with Ar, transferred into an annealing furnace, and annealed at 950 °C for 24 h followed by quenching in ice water. The intermetallic specified above was also modified by oxygen to yield the composition $AB_2O_{0.05}$. The oxygen was introduced by adding $TiO_2$ to the charge, with corresponding decrease of the Ti amount, followed by arc melting and annealing at the same conditions as for oxygen free $AB_2$-type alloy.

The morphology and composition of the alloys were analyzed by SEM and EDS (Hitachi X650). Samples were also characterised by XRD (Bruker D8, Cu–K $\lambda_1$ = 1.5406 Å, $\lambda_2$ = 1.5444 Å, $\lambda_2/\lambda_1$ = 0.5, $2\Theta$ = 20–90°). The XRD data was further processed by Rietveld full-profile analysis using GSAS software.

The $H_2$ absorption kinetics were measured in a Sieverts-type volumetric installation. The measurements were performed at a temperature of 20 °C and hydrogen pressure about 30 bar, for 2 h. The first $H_2$ absorption was performed without activation (after evacuating the sample at the room temperature), after which the sample was activated by heating to 300 °C under vacuum for 1 h.

The PCT studies of the alloys were performed using a commercial automated Sievert-type apparatus (PCT Pro-2000). Roughly, 2 g sample was loaded into the reactor; the sample was then activated by heating to 300 °C under dynamic vacuum for 1 h. The sample was then allowed to cool down to ambient temperature, followed by charging with hydrogen at

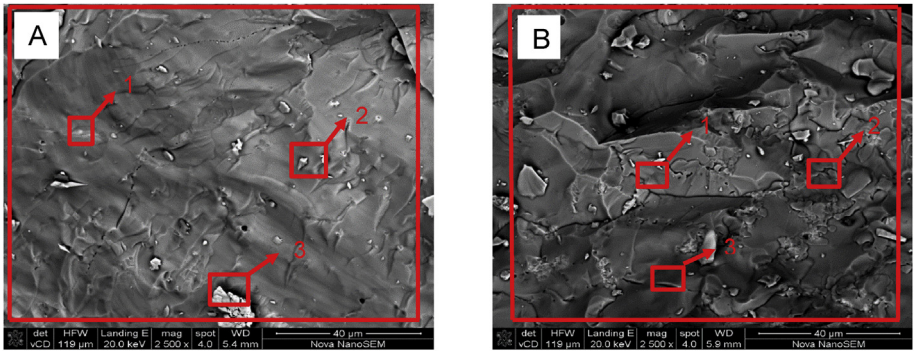


**Fig. 1 – Typical SEM images for the arc-melted samples: (A) $Ti_{0.85}Zr_{0.15}Cr_{0.2}Mn_{1.22}Ni_{0.22}V_{0.3}Fe_{0.06}$, (B) $Ti_{0.85}Zr_{0.15}Cr_{0.2}Mn_{1.22}Ni_{0.22}V_{0.3}Fe_{0.06}O_{0.05}$.**

**Table 1 – Compositional properties of the multi component $AB_2$ type alloys prepared via arc melting.**

| Components | Content, wt% | | | | | | | | | |
|---|---|---|---|---|---|---|---|---|---|---|
| | Nominal | Measured Fig. 1(A) $Ti_{0.85}Zr_{0.15}Cr_{0.2}Mn_{1.22}Ni_{0.22}V_{0.3}Fe_{0.06}$ | | | | Nominal | Measured Fig. 1(B) $Ti_{0.85}Zr_{0.15}Cr_{0.2}Mn_{1.22}Ni_{0.22}V_{0.3}Fe_{0.06}O_{0.05}$ | | | |
| | | Total area | Point 1 | Point 2 | Pont 3 | | Total area | Point 1 | Point 2 | Point 3 |
| A (Ti) | 24.922 | 26.44 | 25.08 | 24.32 | 29.86 | 24.8 | 24.31 | 26.37 | 28.02 | 26.44 |
| A (Zr) | 8.375 | 8.72 | 9.86 | 9.27 | 8.39 | 8.335 | 9.45 | 8.73 | 8.63 | 12.3 |
| B (Cr) | 6.365 | 4.9 | 5.3 | 6.66 | 3.77 | 6.334 | 6.09 | 6.97 | 5.49 | 8.08 |
| B (Mn) | 41.026 | 39.19 | 39.8 | 39.89 | 35.42 | 40.826 | 40.02 | 39.43 | 37.74 | 32.7 |
| B (Ni) | 7.906 | 9.31 | 8.46 | 7.8 | 11.72 | 7.868 | 7.31 | 6.31 | 7.81 | 6.72 |
| B (Fe) | 2.051 | 1.99 | 2.07 | 2.15 | 1.78 | 2.041 | 2.4 | 2.25 | 2.34 | 2.7 |
| B (V) | 9.355 | 9.45 | 9.44 | 8.75 | 9.06 | 9.309 | 9.64 | 8.82 | 9.33 | 10.21 |
| Impurity:(O) | – | – | – | 1.16 | – | 0.487 | 0.78 | 1.12 | 0.64 | 0.85 |

100 bar. The hydrogen absorption and desorption isotherms were recorded at different temperatures 20, 40 and 60 °C and hydrogen pressures from 0.1 to 100 bar. The accuracy of pressure measurements was assumed to be equal to the value (1% of the reading) specified in the instrument documentation while the accuracy of maintaining temperature during taking the isotherms was estimated as a standard deviation of the sample temperature measured during the experiment (±0.1 °C for T = 20 and 40 °C and ±0.3 °C for T = 60 °C). These data were further used to provide error bars in Van't Hoff plots $\ln(P_{EQ}) = F(1/T)$built at hydrogen concentrations which corresponded to plateau midpoint (1 wt% H).

## Results and discussion

The SEM images of the unmodified $AB_2$ and modified $AB_2O_{0.05}$ are shown in Fig. 1. The SEM and EDS analysis shows that both alloys are homogeneous. It can be observed that both alloys have a smooth continuous surface. It can also be seen that the

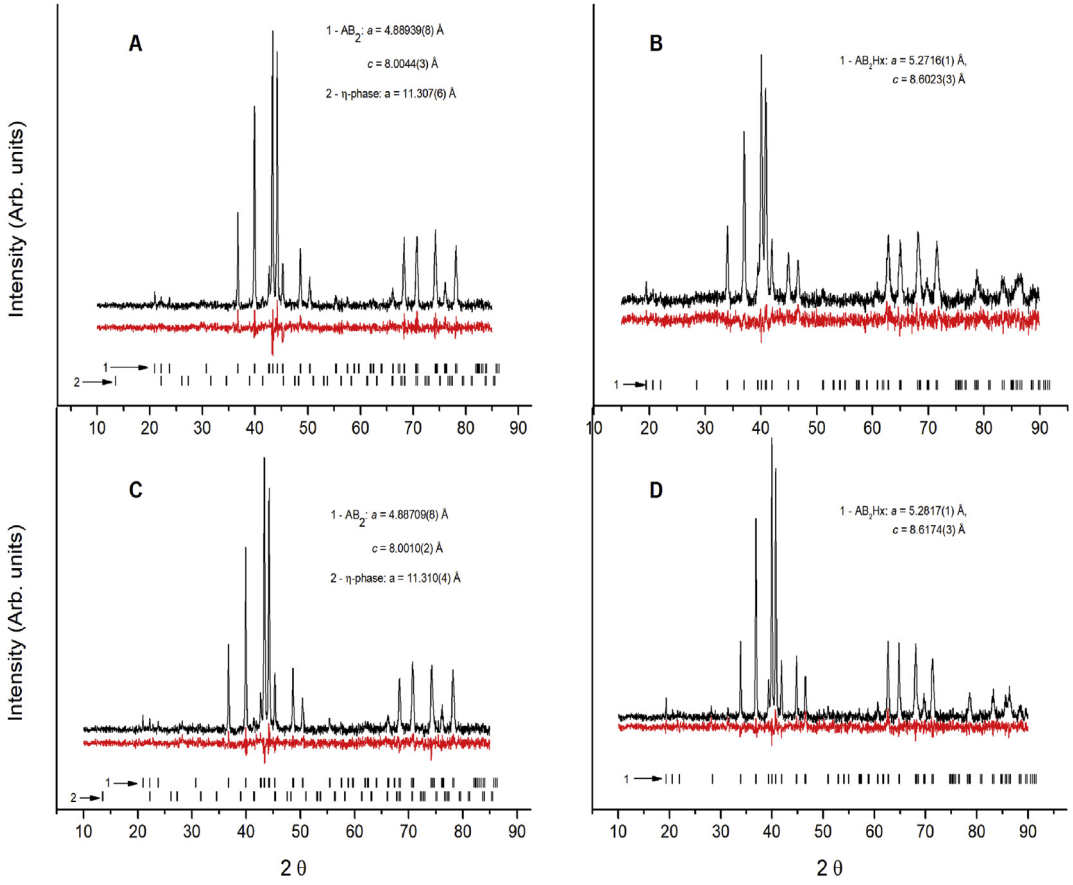


**Fig. 2 – XRD patterns for arc-melted samples (A) as prepared $AB_2$ alloy, (B) hydrogenated $AB_2$ alloy, (C) as prepared $AB_2O_{0.05}$ alloy, (D) hydrogenated $AB_2O_{0.05}$.**

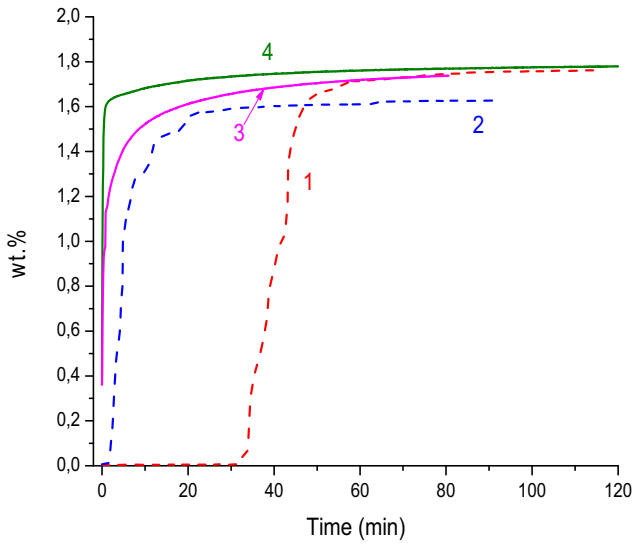


**Fig. 3 – Hydrogen absorption kinetics at T = 20 °C and $P_0$ = 30 bar for the Ti-based $AB_2$ type alloys: (1) $AB_2$ alloy without activation, (2) $AB_2O_{0.05}$ alloy without activation, (3) $AB_2O_{0.05}$ alloy after activation by vacuum heating at 300 °C for 1 h, (4) $AB_2$ alloy after activation by vacuum heating at 300 °C for 1 h.**

oxygen modified sample (Fig. 1 (B)) has more cracks on the surface then the unmodified sample (Fig. 1 (A)). The EDS results shown in Table 1 confirm the XRD data, which displays the main C14-Laves phase with a composition corresponding to A:B ≈ 2, this is confirmed as the measured amounts of the metals correspond closely to the nominal composition of the alloy. EDS results show that the total oxygen impurity was 0.78 wt% for the modified sample (B), while in the unmodified sample (A) oxygen was only detected at point 2, this can be attributed mainly to the use of FeV as it contains small amounts of impurities (see Ref. [23] Which presents results of characterization of the used FeV).

Fig. 2 shows the refined XRD patterns for the as prepared alloys (A, C) and the hydrogenated alloys (B, D). XRD analysis showed that both alloys consist of the main C14 Laves phase ([24], ID: 21,112). Both alloys exhibited impurity of η – phase ($Ti_4Fe_2O_{1-x}$) corresponding to 1.2 and 3.8 wt % respectively, the reason for the appearance of the impurity phase in the unmodified sample (A) is mainly attributed to the use of commercial ferrovanadium. The main constituent of the hydrogenated alloys is a hydride phase $AB_2H_x$ with the increased unit cell volume $\Delta V/V_0 = 24.93\%$ and 25.80%, for the unmodified (Fig. 2 (B)) and oxygen-modified (Fig. 2 (D)) samples, respectively.

The hydrogen absorption kinetics of the unmodified and oxygen-modified Ti based $AB_2$ are illustrated in Fig. 3. It can be seen that despite slightly slower kinetics for $AB_2O_{0.05}$ as compared to oxygen-free $AB_2$ after activation by vacuum heating, it starts to absorb $H_2$ in the non-activated state immediately while the non-activated oxygen-free sample has an incubation period about 30 min. This is mainly due to the occurrence of the η-$(Ti,Zr)_4Fe_2O_{1-x}$ phase in the alloy, which acts as a catalyst for hydrogen absorption; it also increases brittleness of the starting alloy. However, the introduction of oxygen into the alloy leads to a slight decrease in the hydrogen absorption capacity, from 1.8 wt% to 1.7 wt%.

Fig. 4(A) and (B) shows the hydrogen absorption and desorption isotherms of $Ti_{0.85}Zr_{0.15}Cr_{0.2}Mn_{1.22}Ni_{0.22}V_{0.3}Fe_{0.06}$ and for the oxygen modified $Ti_{0.85}Zr_{0.15}Cr_{0.2}Mn_{1.22}Ni_{0.22}V_{0.3}Fe_{0.06}O_{0.05}$ samples at 20, 40 and 60 °C. The isotherms for both samples exhibit the presence of two different phases, namely α-solid solution of hydrogen in the parent intermetallic and β-hydride. The two-phase (α + β) region of hydrogen concentrations is manifested by the appearance of plateau. From the P–C isotherms measurement, the maximum hydrogen storage capacity was approximately 2 wt % at $P(H_2)$ = 90 bar and T = 20 °C for both alloys. The reversible storage capacity for the unmodified $AB_2$ alloy is 1.7 wt% and for the oxygen modified $AB_2$ alloy it is 1.6 wt%. The reason for the slight decrease in the H storage capacity could be due to the formation of hydride of the η-phase which is characterised by a high stability and does not desorb hydrogen at experimental pressure – temperature conditions [17–19].

The formation of the η-phase (A:B = 2:1) may result in the withdrawal of the A component from the major Laves phase making it over-stoichiometric (B/A>2). In turn, it can result in

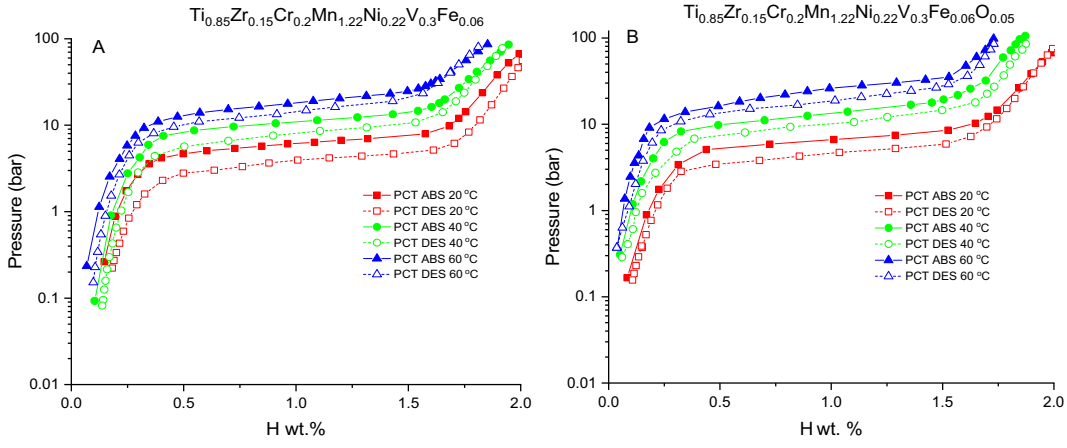


**Fig. 4 – Hydrogen absorption and desorption isotherms for Ti based $AB_2$ alloys (A) Unmodified $AB_2$, (B) Oxygen modified $AB_2$ alloy.**

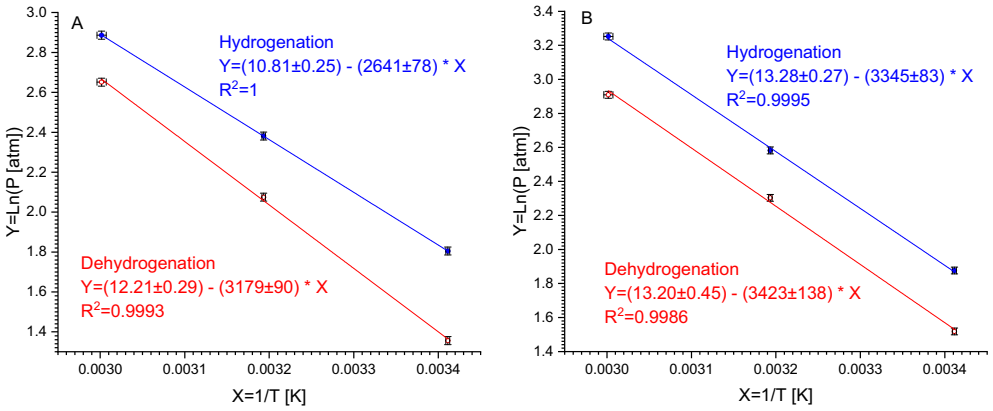


**Fig. 5 – Van't Hoff plots for hydrogen absorption and desorption for the unmodified (A) and modified (B) alloys.**

the decrease of thermal stability of the $AB_2$ hydride. Indeed, the P–C isotherms (Fig. 4) show that the plateau pressures for the oxygen-modified $AB_2$ sample are higher than the unmodified $AB_2$ sample.

The thermodynamic properties such as the enthalpies and entropies of formation and dissociation of the two hydrides were calculated from the Van't Hoff plots shown in Fig. 5(A) and (B). Good linear relationships were observed in the Van't Hoff plots for both alloys. The values for ΔH and ΔS for the unmodified sample obtained from Van't Hoff plots were calculated as −22.0 ± 0.6 kJ/mol $H_2$ and −90 ± 2 J/K/mol $H_2$ for absorption and 26.4 ± 0.7 kJ/mol $H_2$ and 102 ± 2 J/K/mol $H_2$ for desorption; the values for the modified sample are −27.8 ± 0.7 kJ/mol $H_2$ and −110 ± 2 J/K/mol $H_2$ for absorption and 28 ± 1 kJ/mol $H_2$ and 110 ± 4 J/K/mol $H_2$ for desorption.

## Conclusions

The modification of Ti-based $AB_2$ alloy by oxygen introduction was investigated. The results revealed that with the increase of oxygen content in the Ti-based $AB_2$ alloy an increase in the abundance of η – phase ($Ti_4Fe_2O_{1-x}$) impurity occurs. The activation performance of the Ti-based $AB_2$ alloy was improved by the introduction of oxygen into the alloy allowing it to absorb $H_2$ without any activation, but decreases its reversible hydrogen absorption capacity from 1.7 wt% to 1.6 wt%.

## Acknowledgments

This work is funded by South African Department of Science and Technology (DST) within HySA program (projects KP6–S01 and KP6–S03). The international collaboration is supported by the EC, Grant Agreement number: 778307 – HYDRIDE4MOBILITY – H2020-MSCA-RISE-2017. MWD and ML also acknowledge support of National Research Foundation (NRF) of South Africa, grant numbers 116278 (MWD) and 109092 (ML).

## REFERENCES

[1] Lototskyy MV, Tolj I, Pickering L, Sita C, Barbir F, Yartys V. The use of metal hydrides in fuel cell applications. Prog Nat Sci: Mat Inter 2017;27:3–20.
[2] Bellosta von Colbe J, Ares JR, Barale J, Baricco M, Buckley C, Capurso G, et al. Application of hydrides in hydrogen storage and compression: achievements, outlook and perspectives. Int J Hydrogen Energy 2019;44:7780–808.
[3] Hirscher M, Yartys VA, Baricco M, Bellosta von Colbe J, Blanchard D, Bowman Jr RC, et al. Materials for hydrogen-based energy storage – past, recent progress and future outlook. J Alloys Compd 2020;827:153548.
[4] Manickam K, Grant DM, Walker GS. Optimization of $AB_2$ type alloy composition with superior hydrogen storage properties for stationary applications. Int J Hydrogen Energy 2015;40:16288–96.
[5] Pickering L, Lototskyy MV, Davids MW, Sita C, Linkov V. Induction melted $AB_2$-type metal hydrides for hydrogen storage and compression applications. Mater Today: Proceedings 2018;5(4):10470–8.
[6] Zadorozhnyy V, Sarac B, Berdonosova E, Karazehir T, Lassnig A, Gammer C, et al. Evaluation of hydrogen storage performance of ZrTiVNiCrFe in electrochemical and gas-solid reactions. Int J Hydrogen Energy 2020;45:5347–55.
[7] Taizhong H, Wu Z, Xia B, Chen J, Yu X, Xu N, et al. $TiCr_{1.2}(VeFe)_{0.6}$ - a novel hydrogen storage alloy with high capacity. Sci Technol Adv Mater 2003;4:491–4.
[8] Kim JH, Han KS, Hwang KT, Kim BG, Kang YM. Effect of heat treatment on microstructure and hydrogen storage properties of mass-produced $Ti_{0.85}Zr_{0.13}(Fe_x–V)_{0.56}Mn_{1.47}Ni_{0.05}$ alloy. Int J Hydrogen Energy 2013;38:6215–20.
[9] Sakaki K, Kim H, Enoki H, Yoshimura SI, Ino S, Nakamura Y. Development of TiZrMn based hydrogen storage alloys for a soft actuator. Mater Trans 2014;55:1168–74.
[10] Yadav TP, Shahi RR, Srivastava ON. Synthesis, characterization and hydrogen storage behaviour of $AB_2$ ($ZrFe_2$, $Zr(Fe_{0.75}V_{0.25})_2$, $Zr(Fe_{0.5}V_{0.5})_2$ type materials. Int J Hydrogen Energy 2012;37:3689–96.
[11] Zhang YL, Li JS, Zhang TB, Hu R, Xue XY. Microstructure and hydrogen storage properties of non-stoichiometric Zr–Ti–V Laves phase alloys. Int J Hydrogen Energy 2013;34:14675–84.
[12] Chen Z, Xiao X, Chen L, Fan X, Liu L, Li S, Ge H, Wang Q. Influence of Ti super-stoichiometry on the hydrogen storage

properties of $Ti_{1+x}Cr_{1.2}Mn_{0.2}Fe_{0.6}$ (x = 0–0.1) alloys for hybrid hydrogen storage application. J Alloys Compd 2014;585:307–11.
[13] Ulmer U, Dieterich M, Pohl A, Dittmeyer R, Linder M, Fichtner M. Study of the structural, thermodynamic and cyclic effects of vanadium and titanium substitution in laves-phase $AB_2$ hydrogen storage alloys. Int J Hydrogen Energy 2017;42:20103–10.
[14] Chen S-K, Lee P-H, Lee H, Su H-T. Hydrogen storage of C14-$Cr_uFe_vMn_wTi_xV_yZr_z$ alloys. Mater Chem Phys 2018;210:336–47.
[15] Morita Y, Gamo T, Kuranaka S. Effects of nonmetal addition on hydriding properties for Ti–Mn Laves phase alloys. J Alloys Compd 1997;253–254:29–33.
[16] Tsukahara M, Takahashi K, Isomura A, Sakai T. Influence of oxygen on hydrogen storage and electrode properties for micro-designed V-based battery alloys. J Alloys Compd 1998;265:257–63.
[17] Davids MW, Lototskyy M. Influence of oxygen introduced in TiFe-based hydride forming alloy on its morphology, structural and hydrogen sorption properties. Int J Hydrogen Energy 2012;37:18155–62.
[18] Mintz MH, Hadari Z, Dariel MP. Hydrogenation of oxygen-stabilized $Ti_2MO_x$ (M = Fe, Co, Ni; $0 \leq x < 0.5$) compounds. J Less Common Met 1980;74:287–94.
[19] Zavaliy IY. Effect of oxygen content on hydrogen storage capacity of Zr-based η-phases. J Alloys Compd 1999;291:102–9.
[20] Zavaliy I, Wojcik G, Mlynarek G, Saldan I, Yartys V, Kopczyk M. Phase-structural characteristics of $(Ti_{1-x}Zr_x)_4Ni_2O_{0.3}$ alloys and their hydrogen gas and electrochemical absorption–desorption properties. J Alloys Compd 2001;314:124–31.
[21] Zavaliy IY, Denys RV, Koval'chuck IV, Riabov AB, Delaplane RG. Hydrogenation of $Ti_{4-x}Zr_xFe_2O_y$ alloys and crystal structure analysis of their deuterides. Chem Metals Alloys 2009;2:59–67.
[22] Zavaliy IY, Denys RV, Riabov AB, Koval'chuck IV, Lyutyy PY. Crystal structure analysis of the $Ti_3ZrFe_2O_{0.3}D_{6.4}$ and $TiZr_3Fe_2O_{0.3}D_{7.5}$ deuterides. Chem Metals Alloys 2014;7:100–5.
[23] Lototskyy M, Goh J, Davids MW, Linkov V, Khotseng L, Ntsendwana B, Denys R, Yartys VA. Nanostructured hydrogen storage materials prepared by high-energy reactive ball milling of magnesium and ferrovanadium. Int J Hydrogen Energy 2019;44:6687–701.
[24] White PS, Rodgers JR. CRYSTMET: a database of the structures and powder patterns of metals and intermetallics. Acta Crystallogr 2002;B58:343–8.